Geophysical Research Letters

RESEARCH LETTER
10.1029/2019GL084817

Dipole Structure of Mixed Layer Salinity in Response to El Niño-La Niña Asymmetry in the Tropical Pacific

Cong Guan[1,2,3,4,5], Shijian Hu[1,2,4,5], Michael J. McPhaden[6], Fan Wang[1,2,4,5], Shan Gao[1,2,4,5], and Yinglin Hou[1,2,4,5]

[1]Key Laboratory of Ocean Circulation and Waves, Institute of Oceanology, Chinese Academy of Sciences, Qingdao, China, [2]College of Marine Science, University of Chinese Academy of Sciences, Qingdao, China, [3]Institute of Oceanographic Instrumentation, Shandong Academy of Sciences, Qingdao, China, [4]Center for Ocean Mega-Science, Chinese Academy of Sciences, Qingdao, China, [5]Qingdao National Laboratory for Marine Science and Technology, Qingdao, China, [6]NOAA/Pacific Marine Environmental Laboratory, Seattle, WA, USA

Key Points:
- A dipole structure of mixed layer salinity in the western-central equatorial Pacific is a characteristic of El Niño-La Niña asymmetry
- Nonlinear zonal advection plays a dominant role in generating the dipole salinity structure
- The dipole salinity structure has potential effects on the asymmetry of ENSO SST

Supporting Information:
- Figure S1

Correspondence to:
F. Wang,
fwang@qdio.ac.cn

Citation:
Guan, C., Hu, S., McPhaden, M. J., Wang, F., Gao, S., & Hou, Y. (2019). Dipole structure of mixed layer salinity in response to El Niño-La Niña asymmetry in the tropical Pacific. *Geophysical Research Letters*, *46*, 12,165–12,172. https://doi.org/10.1029/2019GL084817

Received 4 AUG 2019
Accepted 13 SEP 2019
Accepted article online 1 OCT 2019
Published online 6 NOV 2019

Abstract The asymmetry of mixed layer salinity (MLS) anomalies in response to El Niño and La Niña events in the tropical Pacific is examined for the first time based on Argo observations and Estimating the Circulation and Climate of the Ocean simulation. The difference of MLS anomalies between El Niño and La Niña shows a dipole structure, with El Niño featuring strong negative salinity anomalies east of 160°E while La Niña shows remarkable positive salinity anomalies west of 160°E. A salinity budget analysis suggests that nonlinear zonal advection plays a dominant role in generating the asymmetric MLS structure. This dipole MLS structure acts to generate a dipole structure of barrier layer thickness and thus likely plays an important role in the development of El Niño–Southern Oscillation asymmetries in sea surface temperature.

Plain Language Summary The El Niño–Southern Oscillation (ENSO) is well known for its great impacts on global climate. Previous studies on the differences between El Niño and La Niña, defined as ENSO asymmetry, focused primarily on temperature, but the differences in salinity between the two ENSO phases and their potential effects on the ENSO asymmetry are relatively unexplored. In this paper, we have for the first time documented salinity differences associated with El Niño-La Niña asymmetry and diagnosed the air-sea processes in controlling these differences based on observations and model simulations. We find a dipole structure exists in mixed layer salinity (MLS) variations between El Niño and La Niña in the western-central equatorial Pacific, with stronger negative MLS anomalies to the east of 160°E during El Niño and stronger positive MLS anomalies to the west of 160°E during La Niña. Based on a salinity budget analysis, the MLS dipole is mostly attributed to the nonlinear zonal advection. This dipole MLS structure in relation to a dipole structure in barrier layer thickness, and their potential to feedback on El Niño and La Niña sea surface temperature asymmetry, is also discussed.

1. Introduction

As the strongest interannual climate variation on the planet, the El Niño–Southern Oscillation (ENSO) has prominent impacts on global climate and its variability (McPhaden et al., 2006). The global consequences of ENSO result from fluctuations in the distribution of heat in the ocean and atmosphere, but salinity variations are also an important element of the ENSO cycle (Schneider, 2004). Modeling studies have suggested that salinity affects stratification in the Pacific warm pool, leads to the development of a barrier layer (BL) between the mixed layer and isothermal layer, and hence plays an active role in ENSO (Lukas & Lindstrom, 1991; Sprintall & Tomczak, 1992). The BL reduces the subsurface entrainment of cooling water into the warmer-mixed layer (Ando & McPhaden, 1997; Maes et al., 2002) and enhances the zonal displacement of the warm pool by increasing the response of a shallower-mixed layer to atmospheric wind forcing (Maes et al., 1997; Vialard et al., 2002; Vialard & Delecluse, 1998a, 1998b).

Large interannual salinity anomalies in response to ENSO events have been attributed to freshwater forcing and ocean current advection (Cronin & McPhaden, 1998; Delcroix et al., 2011; Delcroix & McPhaden, 2002; Singh et al., 2011). Based on Argo, a salinity front and a thick BL are found to have a clear relationship with the zonal displacement of the warm pool east boundary, accompanied with occurrence of warm sea surface temperature (SST) anomalies (Bosc et al., 2009; Maes et al., 2006). Qu et al. (2014) diagnosed the relationship

between salinity effects and ENSO using extended Argo observations and Aquarius satellite data and found that the BL moves eastward during El Niño and westward during La Niña. The BL anomaly between El Niño and La Niña shows a zonal seesaw pattern along the equator across 160°E (Zheng et al., 2014).

It is well known that the El Niño and La Niña events are not symmetric in terms of amplitude, pattern, and temporal evolution (e.g., Deser & Wallace, 1987; Guan et al., 2018; Hoerling et al., 1980; Larkin & Harrison, 2002; McPhaden & Zhang, 2009; Takahashi et al., 2011; Timmermann et al., 2018). Previous studies have mainly focused on dynamical processes involving wind, oceanic currents and thermocline depth variations, and precipitation. In contrast, less attention has been paid to asymmetries in salinity related to El Niño and La Niña events due to a lack of salinity observations in the past, although the importance of salinity in the evolution of ENSO is widely accepted (Zhang et al., 2012; Zhang & Busalacchi, 2009; Zheng & Zhang, 2012, 2015). Extensive Argo observations, satellite salinity, and model-based ocean state estimates allow us to explore the salinity asymmetries related to ENSO in more detail. In the rest of this paper, we will describe the notable salinity differences associated with El Niño-La Niña asymmetry in section 2 and diagnose the air-sea processes controlling these differences based on a detailed salinity budget analysis in section 3, following by a summary and discussion in section 4.

2. Dipole Salinity Structure in Response to El Niño-La Niña Asymmetry

We use gridded Argo salinity and temperature data over 2005–2017 from the Asian Pacific Data Research Center of the International Pacific Research Center (http://apdrc.soest.hawaii.edu/dods/publicdata/ArgoProducts/monthlymean), with a horizontal resolution of 1° × 1° and a time resolution of 1 month. The Fourier low-pass filter with a cutoff period of 13 months is applied to these data to obtain interannual anomalies (Walters & Heston, 1982). Three El Niño (2006–2007, 2009–2010, and 2015–2016) and three La Niña events (2007–2008, 2010–2011, and 2011–2012) are captured during the period (2005–2017) of Argo observations.

Composite analysis of these El Niño and La Niña events is then conducted to illustrate interannual salinity anomalies associated with El Niño and La Niña (Figure 1). Each composite is normalized by the Niño3.4 SST amplitude in the mature phase (defined as the period from November to the following January) of the corresponding composite ENSO event to avoid the potential biases caused by the El Niño-La Niña amplitude asymmetry (Dommenget et al., 2013; Guan et al., 2018; Takahashi et al., 2011; Timmermann et al., 2018). With or without normalization, however, the patterns are very similar (cf. Figures 1 and S1 in the supporting information). During the mature phase of El Niño, the strongest negative sea surface salinity (SSS) anomalies appear in the western-central equatorial Pacific, centered at 175°E with a maximum of −0.4 psu/°C and extending northeast to North America (Figure 1a). In contrast, the strongest positive SSS anomalies occur in the far-western equatorial Pacific during the mature phase of La Niña, centered near 160°E with a maximum exceeding 0.4 psu/°C (Figure 1d). Near the equator averaged between 5°S–5°N, both the negative and positive salinity anomalies are mainly found in the mixed layer above 100 m. These anomalies begin to develop in April and reach their maximum in the following December.

To make clear comparison of these mixed layer salinity (hereafter MLS) anomalies between El Niño and La Niña with respect of location and amplitude, the composite anomalies are added to show their different structures. A prominent dipole structure appears in the mixed layer of western-central equatorial Pacific, characterized by negative anomalies east of 160°E and positive anomalies to the west, with amplitude exceeding 0.2 psu/°C (Figures 1g to 1i). This dipole structure is initiated in the developing phase of ENSO events and reaches its maximum during the mature phase of the events. The dipole structure can also be clearly seen in recent satellite observations (Figures S2 and S3) from the European Space Agency's Soil Moisture and Ocean Salinity (2010–2017) and the National Aeronautics and Space Administration's Soil Moisture Active Passive (2015–2019), with a few detailed spatial differences probably due to their shorter records.

This asymmetric salinity pattern affects the BL difference between El Niño and La Niña, which also exhibits a dipole structure, with positive BL anomalies east of 165°E and negative BL anomalies west of 165°E (Figure 2). The negative salinity anomalies in the east of the dipole contribute to the positive BL thickness anomalies east of 165°E mainly through a shallower-mixed layer (Zheng et al., 2014). The thicker BL will then affect the SST anomalies via positive feedback processes that reduce subsurface entrainment of

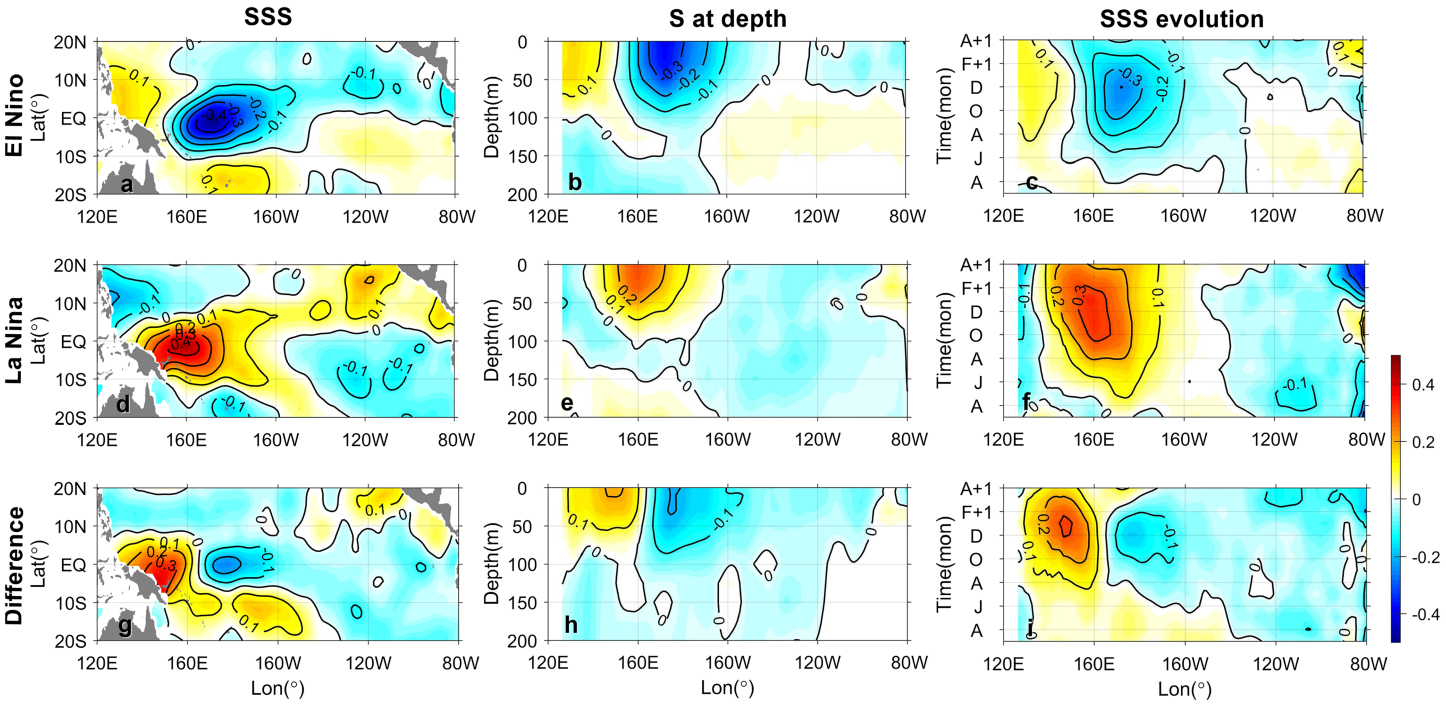

Figure 1. Salinity anomalies for composite El Niño (a–c) and La Niña events (d–f) and their differences (g–i) based on Argo product. SSS anomalies during mature phase are shown in the left panel, salinity averaged between 5S–5N during mature phase is shown in the middle, and evolutions of SSS averaged between 5S–5N are shown in the right. El Niño events for composite include 2006–2007, 2009–2010, and 2015–2016, while La Niñas include 2007–2008, 2010–2011, and 2011–2012. Each composite is normalized by the amplitude of mean Niño3.4 SST anomaly in the corresponding ENSO mature phase based on Argo. For the El Niño events, the Niño3.4 index is 1.57 °C on average, while for La Niña events is 1.28 °C. Unit is in psu/°C. ENSO = El Niño–Southern Oscillation; SSS = sea surface salinity; SST = sea surface temperature.

cooling water and enhance air-sea interactions (e.g., Ando & McPhaden, 1997; Maes et al., 2002; Vialard et al., 2002), contributing to positive SST anomalies east of the dateline (Figure 2f). Similarly, positive salinity anomalies in the western pole of the dipole lead to a thinner BL and hence negative SST anomalies. Therefore, the dipole structures of MLS and BL suggest a role for salinity in the asymmetries of El Niño and La Niña in SST.

Why there is dipole salinity structure? One might expect that this asymmetric salinity patterns might be simply controlled by the ENSO-associated precipitation, since the rain zone will move to the east during El Niño and to the west during La Niña. However, we cannot neglect the effects of advection by ocean currents, which has been suggested by previous studies to the dominant process affecting interannual variability of salinity in the central and western Pacific (Delcroix et al., 2011; Delcroix & McPhaden, 2002; Singh et al., 2011). Therefore, a quantitative analysis is required to clarify the relative importance of these different processes.

3. Salinity Budget Analysis

We will use the Estimating the Circulation and Climate of the Ocean (ECCO) state estimation product, which is based on the Massachusetts Institute of Technology general circulation model (Marshall et al., 1997), to diagnose the salinity budget along the equator in the Pacific over 1993–2016. The ECCO product has been applied in many scientific studies as it validates well against observations of oceanic circulation and water properties (e.g., Ponte & Vinogradova, 2016). Importantly for this study, ECCO conserves energy and mass (e.g., Fukumori et al., 2004; Kim et al., 2004; Qu, 2003; Gao et al., 2014; Zhang et al., 2016).

Before examining the salinity budget, we first compare the salinity output from ECCO with Argo analyses to assess ECCO performance in the tropical Pacific Ocean. The Argo data and ECCO show similar patterns of the long-term mean state of SSS, with a fresh pool (where SSS fresher than 34.5 psu) concentrated in the

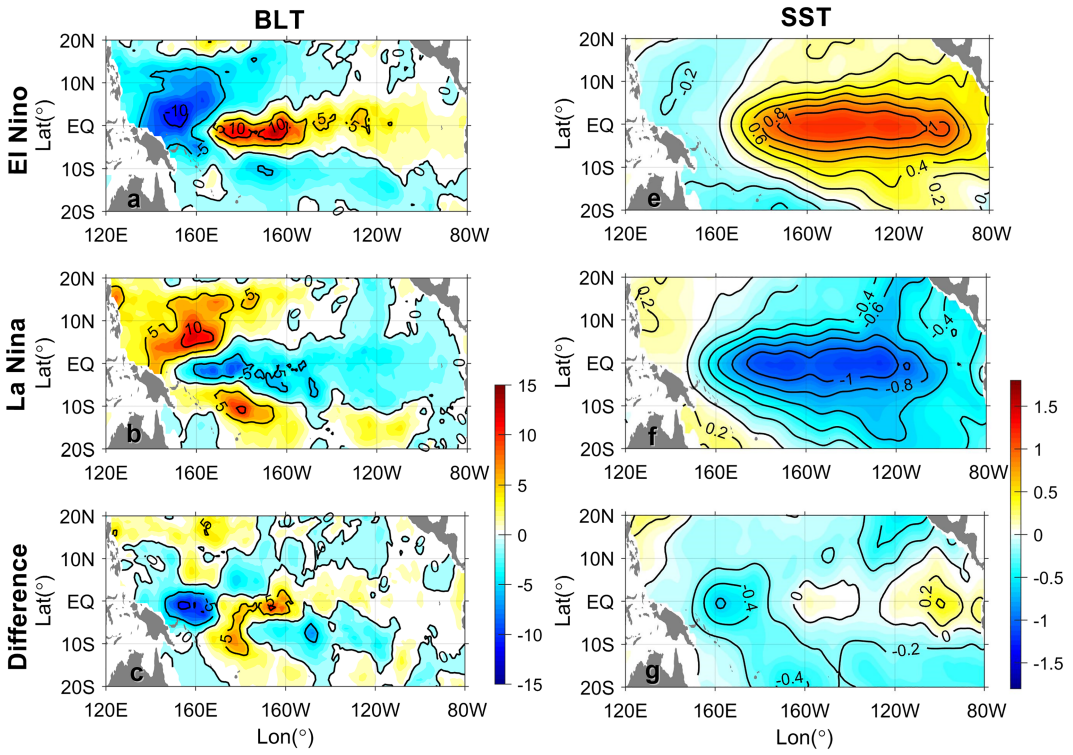

Figure 2. As in Figure 1, but for normalized barrier layer thickness (BLT) anomalies (left) and SST anomalies (right). Units are in m/°C and °C/°C, respectively. SST = sea surface temperature.

western Pacific and two SSS maxima in the northern and southern subtropical gyres (Figures S4 and S5). On interannual time scales, the largest standard deviations are located around 160°E in the western equatorial Pacific, with very similar temporal variations and a correlation coefficient of 0.91 over the period 2005–2016. Furthermore, a similar dipole structure and interannual evolution of MLS are also found based on the ECCO product over both the same period of 2005–2016 as Argo and also an extended period of 1993–2016, except with weaker amplitude and a slight eastward displacement of positive anomalies compared to Argo observations (Figures S6 and S7). Therefore, the ECCO product represents reasonable surface salinity variations in the tropical Pacific and is quite suitable for our salinity budget analysis. Note that the ECCO product used hereafter covers seven El Niño events (with the four more El Niño events than Argo, including 1994–1995, 1997–1998, 2002–2003, and 2004–2005 than Argo) and six La Niña events (including the three more than Argo including 1995–1996, 1998–1999, and 1999–2000).

Following Feng et al. (1998), the salinity diagnostic equation is expressed as

$$\frac{\partial S}{\partial t} = -\frac{S_0(P-E)}{h} - u\frac{\partial S}{\partial x} - v\frac{\partial S}{\partial y} - w_e\frac{S-S_{-h}}{h} + R, \tag{1}$$

where S is the MLS, S_0 is SSS, h is the mixed layer depth defined as the depth at which the density difference is 0.125 g/m^3 greater than the surface salinity, S_{-h} is the salinity right below the mixed layer, P and E are the rates of sea surface precipitation and evaporation, u and v are respectively the zonal and meridional oceanic velocities averaged in the mixed layer, and w_e represents the entrainment velocity as $w_e = dh/dt + w|_{-h}$. The first four terms on the right hand of the equation thus represent surface freshwater flux, zonal advection, meridional advection, and vertical advection, respectively. Unresolved processes such as vertical diffusion and computational errors are contained in the residual R. Interannual anomalies of each budget term are obtained by subtracting the corresponding climatology mean from each term and then filtered by a 13-month Fourier low-pass filter.

Since the salinity dipole structure is most pronounced during the mature phase of ENSO, we make composites of each budget term during the developing phases leading up to the mature phase (defined as the

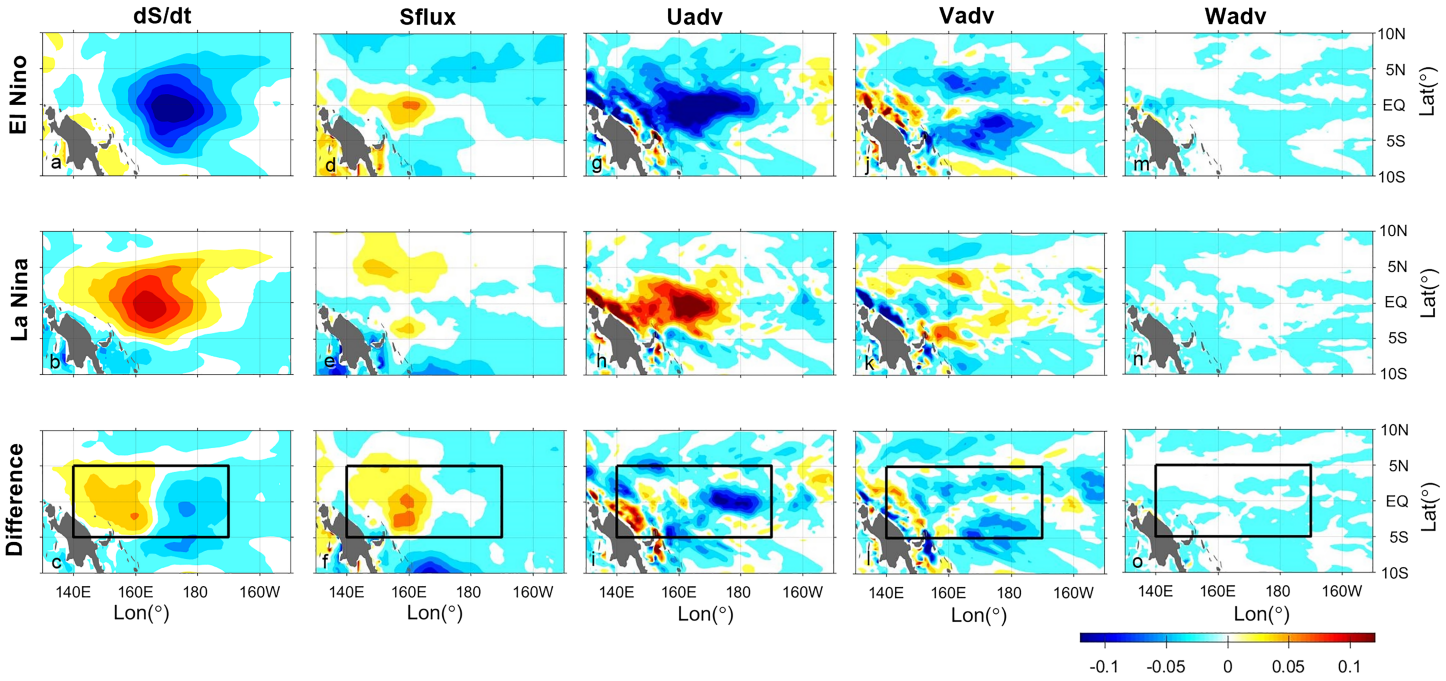

Figure 3. Composite of the terms in the salinity budget during the developing phases of El Niño (a, d, g, j, m), La Niña (b, e, h, k, n), and their attitude difference (c, f, i, l, o) from ECCO. The MLS tendency, tendency caused by surface freshwater flux, zonal advection, meridional advection, and vertical advection, is shown in rows from left to right, respectively. Each composite is normalized by the amplitude of mean Niño3.4 SST anomaly in the corresponding ENSO mature phase based on ECCO. Unit is in psu month^{-1}·°C^{-1}. ECCO = Estimating the Circulation and Climate of the Ocean; ENSO = El Niño–Southern Oscillation; MLS = mixed layer salinity.

averages over the 3 months with maximum MLT tendency) to identify the key processes involved in generating the dipole (Figures 3 and 4).

During the developing phases of El Niño and La Niña events, the patterns of the MLS tendency are mainly consistent with the salinity anomalies during respective ENSO mature phase, with strong negative anomalies centered at 170°E in the equatorial Pacific during El Niño and negative anomalies centered at the 165°E equatorial Pacific in La Niña (Figures 3a and 3b). In contributing to these salinity tendencies, zonal advection (Figures 3g and 3h) has the largest amplitude and therefore plays a dominant role in driving these salinity anomalies during both ENSO warm and cold events (e.g., Delcroix & McPhaden, 2002). During El Niño, surface freshwater flux drives positive MLS anomalies in the western equatorial Pacific due to reduced precipitation and freshens the ocean in the mean intertropical convergence zone and South Pacific convergence zone bands; conversely, freshwater flux contributes to positive MLS anomalies in the off-equatorial western Pacific during La Niña (Figures 3d and 3e). Meridional advection contributes to the MLS tendency mostly in regions around 5° off the equator but damps the tendency on the equator in both El Niño and La Niña events. Vertical advection from the base of the mixed layer is very weak and can be neglected in both ENSO warm and cold events.

In response to the salinity difference between El Niño and La Niña developing phases, the MLS tendency also exhibits a similar dipole structure in the western-central equatorial Pacific (marked within a box covering 140°E–170°W, 5°S–5°N; Figure 3c), featured by positive anomalies to the west of 165°E and negative anomalies to the east. Among the budget terms, it is found that only zonal advection shows a clear dipole structure in line with the MLS tendency (Figure 3i). The surface freshwater flux makes its largest positive contribution in the west but makes nearly no contribution to the east equatorial region. The difference in meridional advection is mainly negative in the boxed region and the difference in vertical advection is weak.

Considering the dominant role of zonal advection, we break up u and $\frac{\partial S}{\partial x}$ into their climatological means and monthly anomalies such that the zonal advection term can be decomposed into three parts as $\left(-u\frac{\partial S}{\partial x}\right)' = -$

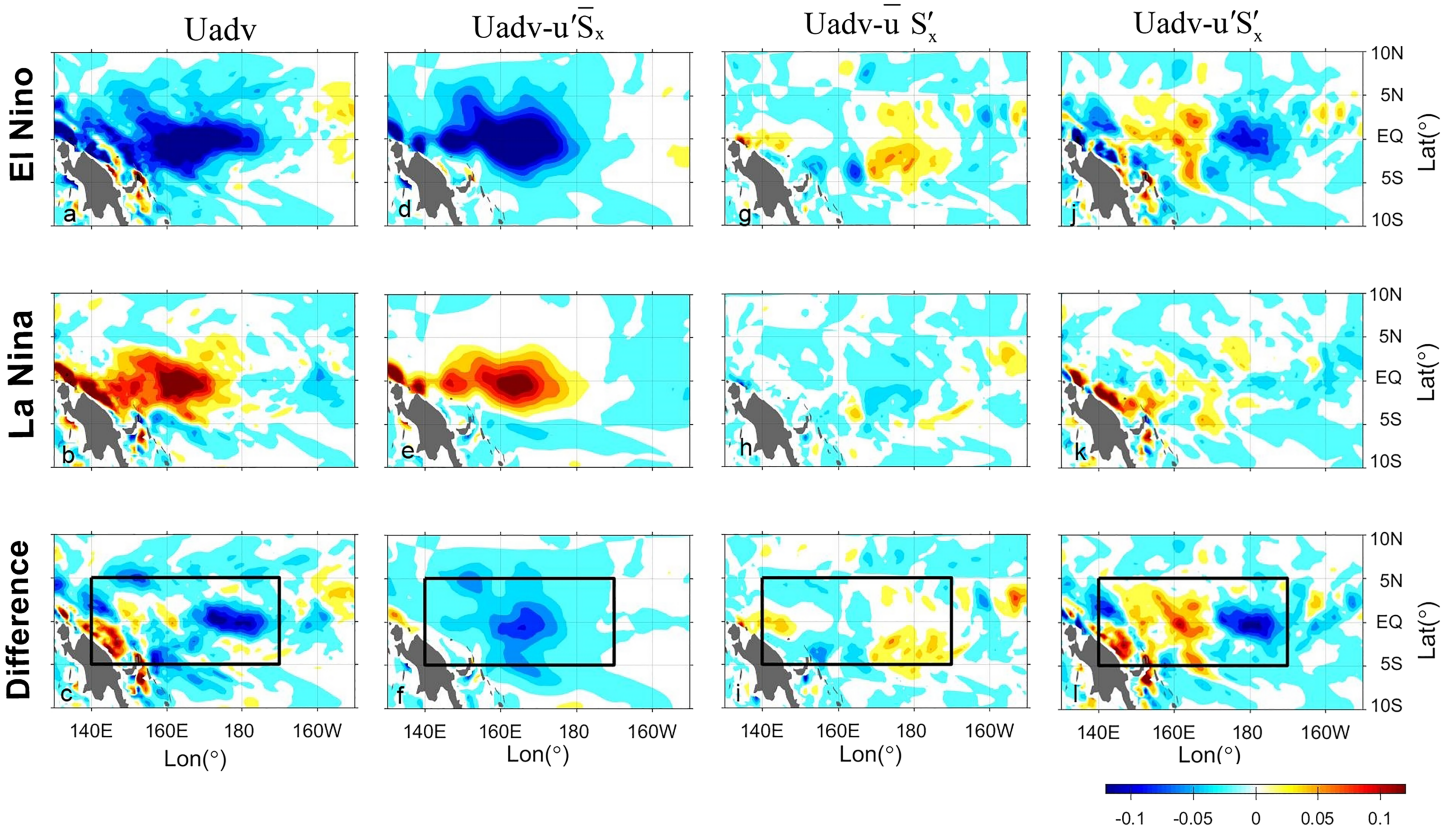

Figure 4. As in Figure 3, but for the decomposition of the MLS tendency caused by zonal advection, which are respectively induced by anomalous zonal current, zonal gradient of MLS anomaly, and the nonlinear process. MLS = mixed layer salinity.

$u'\frac{\partial \overline{S}}{\partial x}-\overline{u}\frac{\partial S'}{\partial x}-u'\frac{\partial S'}{\partial x}$, which are respectively anomalous advection of the mean zonal salinity gradient, mean zonal advection of the anomalous MLS gradient, and the nonlinear advection. Interannual anomalies are then computed as stated above. We find that advection by the anomalous zonal current plays a dominant role in the development of the respective El Niño and La Niño salinity anomalies (e.g., Delcroix & McPhaden, 2002); however, its difference shows a negative tendency in the boxed region due to a stronger zonal advection in El Niño than La Niña events and thus does not contribute to the dipole structure of salinity variations (Figures 4d and 4f). Mean advection of the anomalous salinity gradient has mainly an opposite pattern to the dipole MLS tendency. Interestingly, we find that a clear dipole structure appears in the nonlinear zonal advection term (Figure 4l), similar to the sum of zonal advection, indicating its dominant role in producing the dipole structure of MLS tendency.

Therefore, we conclude that the dipole structure of MLS in the western-central equatorial Pacific between El Niño and La Niña during their respective developing phases results mainly from asymmetric changes in nonlinear zonal advection.

4. Summary and Discussion

In this paper, characteristics of tropical Pacific salinity anomalies related to the El Niño-La Niña asymmetry have been explored using the Argo observations and ECCO ocean state estimates. We find that a dipole structure of salinity difference occurs in the mixed layer of the western-central equatorial Pacific between El Niño and La Niña, with negative SSS anomalies to the east of 160°E and positive SSS anomalies to the west. This salinity dipole structure occurs in the developing phases of El Niño and La Niña. The similar dipole structure in BL thickness and SST anomalies in the central-western Pacific suggests a potential role for the salinity dipole in the development of the SST asymmetry between El Niño and La Niña events.

Based on a salinity budget analysis, we examined the processes that give rise to the dipole structure in salinity anomalies. A clear dipole structure is also found in the mixed layer salinity tendency with its largest amplitude during ENSO developing phases. The main mechanism responsible for this dipole structure is the asymmetry of nonlinear zonal advection between El Niño and La Niña, neither the direct effect of surface freshwater flux nor anomalous zonal advection for the mean salinity gradient.

This raises the question of what dynamical processes lie behind the asymmetry of nonlinear zonal advection. The nonlinear term includes variations in zonal velocity and zonal salinity gradient. Previous studies have suggested that Madden–Julian oscillation events can drive both anomalies of precipitation and zonal wind in the western Pacific during the developing phases of ENSO events (Matthews et al., 2010, Drushka et al., 2012). However, our analysis from ECCO is based on monthly time series products and so these higher-frequency variations are largely filtered out. Thus, asymmetric nonlinear advection is most likely related to the low-frequency nonlinear variations in the zonal oceanic velocity and precipitation, the latter of which affects the zonal salinity gradient. This dipole in SSS is reflected in a dipole in BL thickness, which may contribute to asymmetric SST variations and feedbacks from the ocean to the atmosphere over the ENSO cycle.

Acknowledgments
We thank the two anonymous reviewers for their constructive comments on the original version of this manuscript. C. G. was supported by the National Natural Science Foundation of China (Grants 41806016 and 41730534) and the China Postdoctoral Science Foundation (Grant 2017M622289). S. H. was supported by the National Natural Science Foundation of China (Grants 41776018 and 91858101). The Argo product is available at FNMOC's Argo data sever (http://ftp//usgodael.fnmoc.navy.mil/pub/outgoing/argo/) and the ECCO product is applied from JPL's ECCO data server (http://ecco.jpl.nasa.gov/external/). This is PMEL contribution no. 4996.

References

Ando, K., & McPhaden, M. J. (1997). Variability of surface layer hydrography in the tropical Pacific Ocean. *Journal of Geophysical Research*, *102*(C10), 23,063–23,078.

Bosc, C., Delcroix, T., & Maes, C. (2009). Barrier layer variability in the western Pacific warm pool from 2000 to 2007. *Journal of Geophysical Research*, *114*, C06023. https://doi.org/10.1029/2008JC005187

Cronin, M. F., & McPhaden, M. J. (1998). Upper ocean salinity balance in the western equatorial Pacific. *Journal of Geophysical Research*, *103*(C12), 27,567–27,587.

Delcroix, T., Alory, G., Cravatte, S., Corrège, T., & McPhaden, M. J. (2011). A gridded sea surface salinity data set for the tropical pacific with sample applications (1950-2008). *Deep-Sea Research Part I: Oceanographic Research Papers, 58*(1), 38–48.

Delcroix, T., & McPhaden, M. (2002). Interannual sea surface salinity and temperature changes in the western Pacific warm pool during 1992–2000. *Journal of Geophysical Research*, *107*(C12), 8002. https://doi.org/10.1029/2001JC000862

Deser, C., & Wallace, J. M. (1987). El Niño events and their relation to the Southern Oscillation: 1925–1986[J]. *Journal of Geophysical Research*, *92*(C13), 14,189–14,196.

Dommenget, D., Bayr, T., & Frauen, C. (2013). Analysis of the non-linearity in the pattern and time evolution of El Niño southern oscillation. *Climate Dynamics*, *40*, 2825–2847.

Drushka, K., Sprintall, J., Gille, S. T., & Wijffels, S. (2012). In situ observations of madden-julian oscillation mixed layer dynamics in the indian and western pacific oceans. *Journal of Climate*, *25*(25), 2306–2328.

Feng, M., Hacker, P., & Lukas, R. (1998). Upper ocean heat and salt balances in response to a westerly wind burst in the western equatorial Pacific during TOGA COARE. *Journal of Geophysical Research*, *103*(C5), 10,289–10,311.

Fukumori, I., Lee, T., Cheng, B., & Menemnlis, D. (2004). The origin, pathway, and destination of Nino-3 water estimated by a simulated passive tracer and its adjoint. *Journal of Physical Oceanography*, *34*, 582–604. https://doi.org/10.1175/2515.1

Gao, S., Qu, T., & Nie, X. (2014). Mixed layer salinity budget in the tropical Pacific Ocean estimated by a global GCM. *Journal of Geophysical Research: Oceans*, *119*, 8255–8270, https://doi.org/10.1029/2004GL021142.

Guan, C., McPhaden, M. J., Wang, F., & Hu, S. (2018). Quantifying the role of oceanic feedbacks on ENSO asymmetry. *Geophysical Research Letters*, *46*, 2140–2148.

Hoerling, M. P., Kumar, A., & Zhong, M. (1980). El Niño, La Niña, and the nonlinearity of their teleconnections. *Journal of Climate.*, *10*(10), 1769–1786.

Kim, S. B., Lee, T., & Fukumori, I. (2004). The 1997-1999 abrupt change of the upper ocean temperature in the north-central Pacific. *Geophysical Research Letters*, *31*, L22304, https://doi.org/10.1029/2004GL021142.

Larkin, N. K., & Harrison, D. (2002). ENSO warm (El Niño) and cold (La Niña) event life cycles: Ocean surface anomaly patterns, their symmetries, asymmetries, and implications. *Journal of Climate*, *15*(10), 1118–1140.

Lukas, R., & Lindstrom, E. (1991). The mixed layer of the western equatorial Pacific Ocean. *Journal of Geophysical Research Oceans*, *96*, 3343–3357.

Maes, C., Ando, K., Delcroix, T., Kessler, W. S., McPhaden, M. J., & Roemmich, D. (2006). Observed correlation of surface salinity, temperature and barrier layer at the eastern edge of the western Pacific warm pool. *Geophysical Research Letters*, *33*, L06601. https://doi.org/10.1029/2005GL024772

Maes, C., Delecluse, P., & Madec, G. (1997). Impact of westerly wind bursts on the warm pool of the TOGA-COARE domain in an OGCM. *Climate Dynamics*, *14*, 55–70.

Maes, C., Picaut, J., & Belamari, S. (2002). Salinity barrier layer and onset of El Nino in a Pacific coupled model. *Geophysical Research Letters*, *29*(24), 2206, https://doi.org/10.1029/2002GL016029

Marshall, J., Adcroft, A., Hill, C., Perelman, L., & Heisey, C. (1997). A finite-volume, incompressible Navier Stokes model for studies of the ocean on parallel computers. *Journal of Geophysical Research*, *102*, 5753–5766.

Matthews, A. J., Singhruck, P., & Heywood, K. J. (2010). Ocean temperature and salinity components of the Madden-Julian oscillation observed by Argo floats. *Climate Dynamics*, *35*(7), 1149–1168.

McPhaden, M. J., Zebiak, S. E., & Glantz, M. H. (2006). ENSO as an integrating concept in Earth science. *Science*, *314*, 1740–1745.

McPhaden, M. J., & Zhang, X. (2009). Asymmetry in zonal phase propagation of ENSO sea surface temperature anomalies. *Geophysical Research Letters*, *36*, L13703. https://doi.org/10.1029/2009GL038774

Ponte, R. M., & Vinogradova, N. T. (2016). An assessment of basic processes controlling mean surface salinity over the global ocean. *Geophysical Research Letters*, *43*, 7052–7058. https://doi.org/10.1002/2016GL069857

Qu, T. (2003). Mixed-layer heat balance in the western North Pacific. *Journal of Geophysical Research*, *108*(C7), 3242. https://doi.org/10.1029/2002JC001536

Qu, T., Song, Y. T., & Maes, C. (2014). Sea surface salinity and barrier layer variability in the equatorial Pacific as seen from Aquarius and Argo. *Journal of Geophysical Research: Oceans.*, *119*, 15–29. https://doi.org/10.1002/2013JC009375

Schneider, N. (2004). The response of tropical climate to the equatorial emergence of spiciness anomalies. *Journal of Climate*, *17*(5), 1083–1095.

Singh, A., Delcroix, T., & Cravatte, S. (2011). Contrasting the flavors of El Niño-Southern Oscillation using sea surface salinity observations. *Journal of Geophysical Research*, *116*, C06016. https://doi.org/10.1029/2010JC006862

Sprintall, J., & Tomczak, M. (1992). Evidence of the barrier layer in the surface layer of the tropics. *Journal of Geophysical Research*, *97*(C5), 7305–7316.

Takahashi, K., Montecinos, A., Goubanova, K., & Dewitte, B. (2011). ENSO regimes: Reinterpreting the canonical and Modoki El Nino. *Geophysical Research Letters*, *38*, L10704. https://doi.org/10.1029/2011GL047364

Timmermann, A., An, S., Kug, J. S., Jin, F. F., Cai, W., Capotondi, A., et al. (2018). El Niño-Southern Oscillation complexity. *Nature*, *559*, 535–545.

Vialard, J., & Delecluse, P. (1998a). An OGCM study for the TOGA decade. Part I: Role of salinity in the physics of the western Pacific fresh pool. *Journal of Physical Oceanography*, *28*, 1071–1088.

Vialard, J., & Delecluse, P. (1998b). An OGCM study for the TOGA decade. Part II: Barrier-layer formation and variability. *Journal of Physical Oceanography*, *28*, 1089–1106.

Vialard, J., Delecluse, P., & Menkes, C. (2002). A modeling study of salinity variability and its effects in the tropical Pacific Ocean during the 1993–1999 period. *Journal of Geophysical Research*, *107*(C12), SRF6-1–SRF6-14. https://doi.org/10.1029/2000JC000758

Walters, R. A., & Heston, C. (1982). Removing tidal-period variations from time-series data using low-pass digital filters. *Journal of Physical Oceanography*, *12*, 112–115.

Zhang, R.-H., & Busalacchi, A. J. (2009). Freshwater flux (FWF)-induced oceanic feedback in a hybrid coupled model of the tropical Pacific. *Journal of Climate*, *22*, 853–879.

Zhang, R.-H., Zheng, F., Zhu, J. S., Pei, Y. H., Zheng, Q. N., & Wang, Z. G. (2012). Modulation of El Niño-Southern Oscillation by freshwater flux and salinity variability in the tropical Pacific. *Advances in Atmospheric Sciences*, *29*, 647–660.

Zhang, Y., Du, Y., Zhang, Y., & Gao, S. (2016). Asymmetry of upper ocean salinity response to the Indian Ocean dipole events as seen from ECCO simulation. *Acta Oceanologica Sinica*, *35*(7), 42–49.

Zheng, F., & Zhang, R. H. (2015). Interannually varying salinity effects on ENSO in the tropical Pacific: A diagnostic analysis from Argo. *Ocean Dynamics*, *65*(5), 691–705.

Zheng, F., & Zhang, R.-H. (2012). Effects of interannual salinity variability and freshwater flux forcing on the development of the 2007/08 La Niña event diagnosed from Argo and satellite data. *Dynamics of Atmospheres and Oceans*, *57*, 45–57.

Zheng, F., Zhang, R.-H., & Zhu, J. (2014). Effects of interannual salinity variability on the barrier layer in the western-central equatorial Pacific: A diagnostic analysis from Argo. *Advances in Atmospheric Sciences*, *31*(3), 532–542.